



# SAPP XXII

22<sup>nd</sup> Symposium on Application of Plasma Processes  
and  
11<sup>th</sup> EU-Japan Joint Symposium on Plasma  
Processing

Book of Contributed Papers

Štrbské Pleso, Slovakia  
18-24 January, 2019

Edited by V. Medvecká, J. Országh, P. Papp, Š. Matejčík



Book of Contributed Papers: 22<sup>nd</sup> Symposium on Application of Plasma Processes and 11<sup>th</sup> EU-Japan Joint Symposium on Plasma Processing, Štrbské Pleso, Slovakia, 18-24 January 2019.

Symposium organised by Department of Experimental Physics, Faculty of Mathematics, Physics and Informatics, Comenius University in Bratislava and Society for Plasma Research and Applications in hotel SOREA TRIGAN\*\*\*, Štrbské Pleso, Slovakia, 18-24 January 2019.

Editors: V. Medvecká, J. Országh, P. Papp, Š. Matejčík

Publisher: Department of Experimental Physics, Faculty of Mathematics, Physics and Informatics, Comenius University in Bratislava; Society for Plasma Research and Applications in cooperation with Library and Publishing Centre CU, Bratislava, Slovakia

Issued: January 2019, Bratislava, first issue

Number of pages: 386

URL: <http://neon.dpp.fmph.uniba.sk/sapp/>

# INVESTIGATION OF THE ELECTROSPRAYED WATER MICRODROPLETS USING OPTICAL IMAGING METHODS

Mostafa Hassan<sup>1</sup>, Mário Janda<sup>1</sup>, Zdenko Machala<sup>1</sup>

<sup>1</sup>*Faculty of Mathematics, Physics and Informatics, Comenius University, Bratislava, Slovakia*

E-mail: Mostafa.Hassan@uniba.sk

Two optical imaging methods for investigating electrospayed water microdroplets interacting with atmospheric air corona discharge plasma were tested: double planar laser beam technique and fast camera imaging. The size distributions of the sprayed microdroplets measured by the two methods did not correlate well due to the lower limit of the camera imaging method. For 13 kV applied across 15.8 mm gap, the most abundant microdroplets were with size 20-30  $\mu\text{m}$ . Further work is needed to improve the spatial resolution of the two methods and be able to detect droplets below 20  $\mu\text{m}$ .

## 1. Introduction

Because of producing large quantities of reactive oxygen and nitrogen species (RONS) that seem to be the most efficient biocidal agents in bio-decontamination by plasma, atmospheric air plasmas generated in contact with water become a great interest in the plasma decontamination community [1]. Plasma activation of liquid droplets of a few to hundreds of microns size address transport limits where the higher surface area to volume ratio enables for rapid solvation of plasma activated species while small volume enables rapid mixing even if only by diffusion [2]. The transport phenomena of various RONS which have various Henry's law solubility coefficients are determined by the water droplet size or layer thickness. An efficient way of producing Plasma activated water is applying water electro spray to fine aerosol droplets through the active plasma region, which results in an efficient transfer of gaseous RONS into water [3]. So, it is important to study the transport mechanism of the plasma reactive species into water droplets of various sizes, as well as the liquid chemistry to better understand the relevant effects of plasmas in liquids or the activity of plasma activated water. Our approach presented here is focused on measuring and controlling the electro-sprayed water droplet size and density. We employ various optical imaging methods. Understanding the plasma reactive species transport into the water as a function of the microdroplet size and density is our key objective with applications in biomedicine, environmental sciences and agriculture. Scarce numerical modeling studies [4,5] of plasma induced RONS transport processes into water will be then supported by experimental measurements.

## 2. Experiment Setup

The experimental setup is shown in Fig. 1 consists of a high voltage power supply and syringe pump which passes the deionized water (with conductivity  $<3 \mu\text{S/cm}$ ) through a plastic tube with a flow rate 0.1 mL/min into a stainless-steel needle (nozzle) electrode with the outer diameter 0.7 mm, opposite to a stainless-steel rounded wire grounded electrode, with a gap distance 15.8 mm. Two diode laser beams (red and green) pass through cylindrical lenses, become planar and then intersect with the droplets sprayed from the needle electrode. The red laser is 5.6 mm below nozzle and above the green laser, which is 10.5 mm below nozzle. The output signals of the laser beams are detected using photodetectors and processed by a digital oscilloscope TEKTRONIX TBS2104. The droplets passing through the two planar laser beams cause a signal decrease, which is proportional to the shaded area of the beam signal on the photodetectors.

A digital camera type CASIO EXILIM is used as complementary imaging of the droplets, with typical record parameters 60 fps (frame per second) shutter speed 40,000 (exposure time  $1/40000 \text{ s} = 25 \mu\text{s}$ ). In order to improve the spatial resolution of the camera, the droplets are illuminated with a strong white LED and the image of droplet shades is magnified using a convex lens and projected onto a white paper screen. The photos are then processed and analyzed by some software Microsoft Office Picture Manager and GIMP.

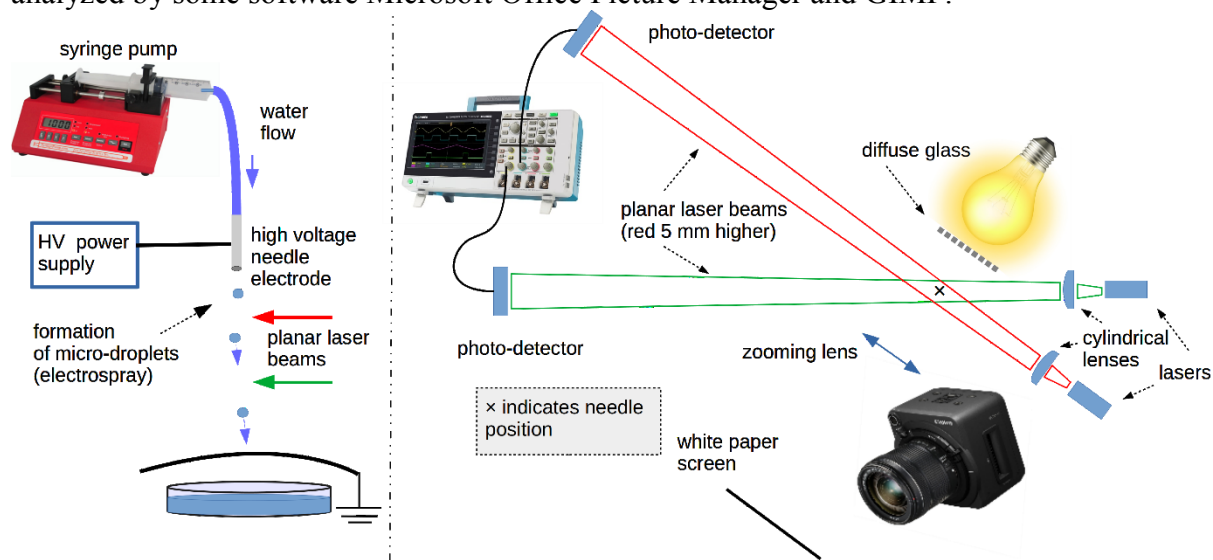


Fig. 1. Experimental Setup.

### 3. Results and Discussion

The electrospayed water microdroplets were measured at several applied positive voltages (5-13 kV) on the needle electrode using the two parallel laser beams and the camera. The horizontal width of the microdroplets was calculated from the laser shading signal, as well as from the photograph sequences. The measured “apparent” vertical height of the droplets is strongly affected by their speed versus the temporal resolution of the laser systems and camera exposure time, as they propagate by accelerated motion in the vertical electric field between the electrode. The visualization of microdroplets by the fast camera was used to calculate the width of the microdroplets and the recorded photos also help us to understand the laser signal waveforms.

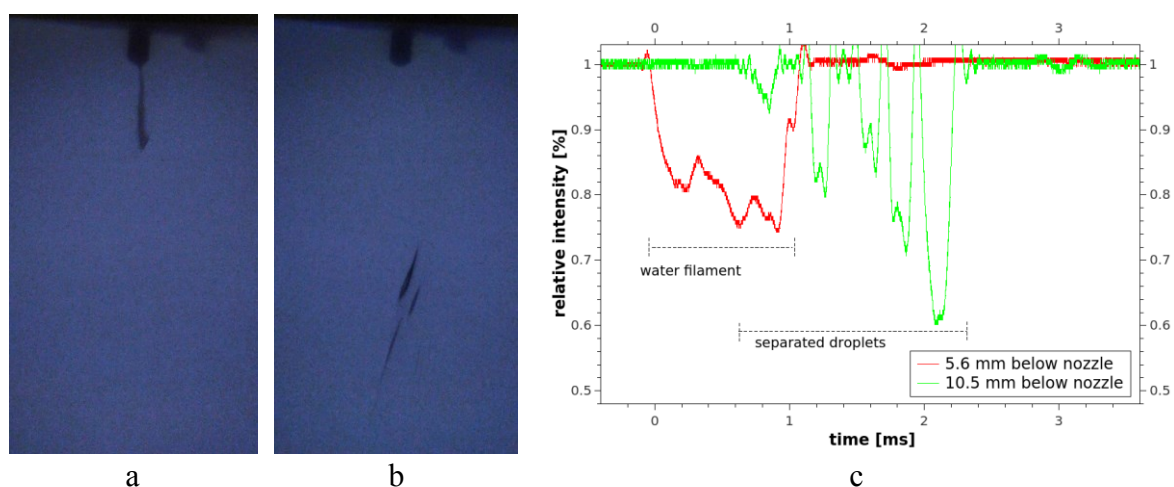


Fig. 2. Microdroplets photographs (exposure time 25  $\mu\text{s}$ ) and corresponding laser beam signals at 13 kV.

Fig. 2a shows the formation of the water filament at the needle nozzle. After the detachment, the filament splits into several microdroplets with widths (38-93)  $\mu\text{m}$  as shown in Fig. 2b. The process of filament elongation and the subsequent formation of droplets can be observed on the temporal evolution of the lasers' intensities  $I$ , as shown in Fig. 2c. The intensity of the upper red laser (5.6 mm below nozzle) decreases as the water filament passes through this planar laser and this intensity decrease is more or less constant for a time interval  $\sim 1$  ms. The signal from the lower laser ( $\sim 10.5$  mm below the nozzle) is different. The filament separation and formation of droplets can be observed as several sharp signal drops in the laser intensity. The individual drops with different minimum values correspond to the microdroplets with different sizes. The smallest (in width) and the fastest microdroplet appears first, while the biggest and the slowest is the last one.

The diameter  $d$  of these droplets is estimated based on the following assumptions. The relative decrease of light intensity  $\Delta I/I_0$  is directly proportional to the ratio of droplet shadow size  $S$  and the detector active area  $A$ . The active area of detectors is given by horizontally oriented optical slit with length  $s_l = 3$  mm and the slit width  $s_w = 100$   $\mu\text{m}$  or  $150$   $\mu\text{m}$ , for green and red laser detectors, respectively. We also consider the horizontal divergence of the planar beams. Due to this divergence, the shadow of the droplets is zoomed in a horizontal plane by a factor  $z_f = 4.7$  or  $3.8$ , for the green and red laser, respectively. We further assume ideal spherical droplets.

Due to the horizontal zoom, the shadow of spherical droplets should be elliptical, with the area

$$S = \pi/4 \times z_f \times d^2 \quad (1)$$

For droplets with  $d < s_w$ , we can thus estimate  $d$  using the following formula

$$d = (4/\pi \times A/z_f \times \Delta I/I_0)^{1/2} \quad (2)$$

The shadow of larger droplets is never entirely projected onto the detector entrance slit. For  $d > 4s_w$ , we can consider the covered area to be rectangular with area  $S = s_w \times z_f \times d$ . For droplets with  $d \in \langle s_w, 4s_w \rangle$ , we introduced a correction factor  $c_f$  so that we can finally estimate the size of droplets as

$$d = A/(z_f \times s_w) \times \Delta I/I_0 + c_f \quad (3)$$

The  $c_f$  decreased linearly from maximum value (for  $d = s_w$ ) down to 0 for  $d = 4s_w$ . The maximum value of  $c_f$  was chosen so that for  $d = s_w$  formulae (2) and (3) give the same result. In practice, we first estimated the diameter of all droplets using eq (2). Then we calculated new diameter for droplets with  $d > s_w$  by eq (3) without the correction factor. Next, we added  $c_f$  to meet the criterion mentioned above. Next, we recalculated the diameter of droplets with  $d > s_w$  using formula (3) with the appropriate correction factor.

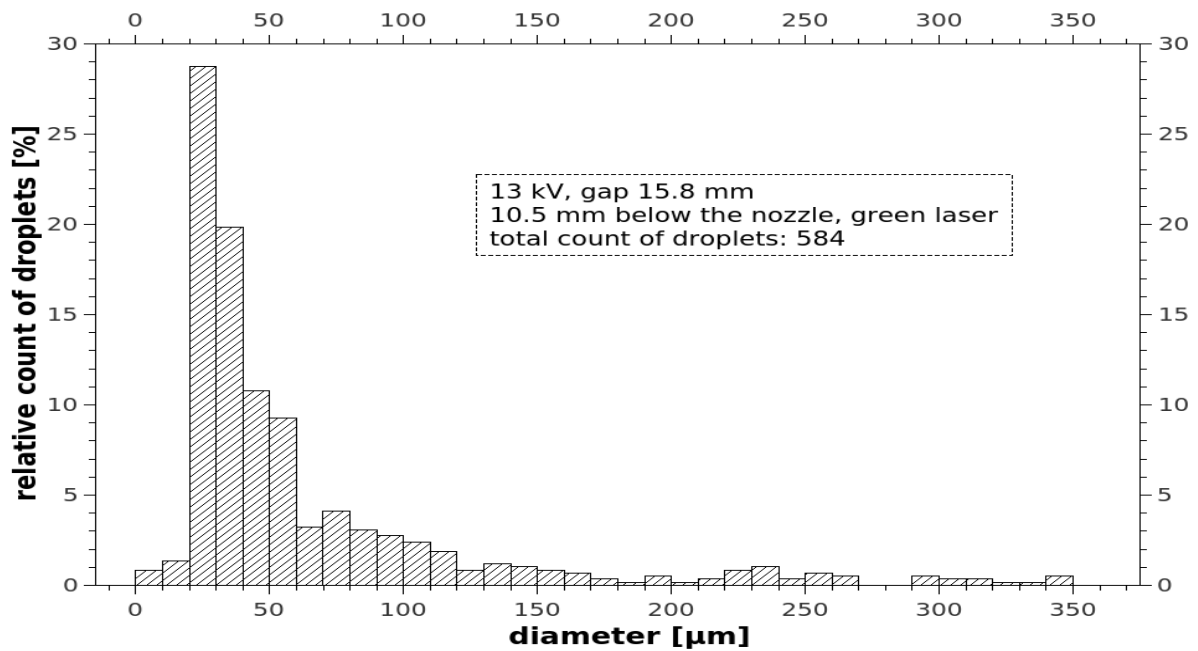


Fig. 3. Droplet size distribution measured by lower green laser 10.5 mm below nozzle, 13 kV.

After analysis of several waveforms, we were able to create a histogram showing the droplet size distribution. Fig. 3 shows the droplet size distribution as measured by the lower green laser in electro spray at 13 kV, with the glow corona discharge. We assume that due to the sensitivity limit, our method underestimates the number of droplets with diameter below 20 μm and that the detection limit is slightly below 10 μm. The most abundant are droplets with  $d = 20\text{-}30\ \mu\text{m}$ .

In order to verify the reliability of this technique we compared the obtained droplet size distribution with that measured from the camera image sequences as shown in Fig. 4. However, based on the camera images, the most abundant droplets are with  $d = 50\text{-}120\ \mu\text{m}$ . We assume that our current camera imaging set-up does not allow us to correctly detect all droplets with diameter below ~50 μm. With the aperture fully opened, our depth of field is narrow, and the image of the droplets is sharp enough only if they do not deviate from the focusing plane. With smaller aperture, we are unable to detect anything with the exposure time as short as 25 μs, due to insufficient illumination and longer exposure times make elongated droplet images as they move in the electric field. We thus cannot reliably compare the results obtained by the two presented techniques now.

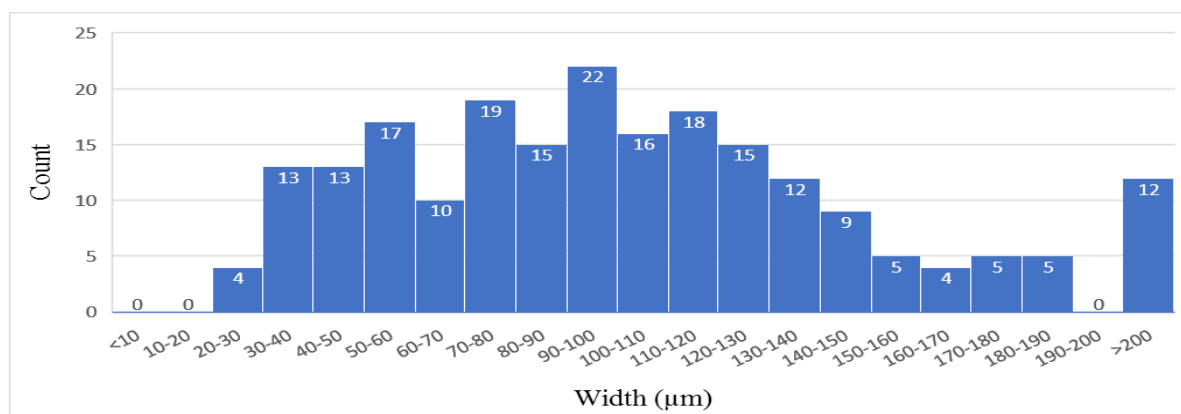


Fig. 4. Size distribution of microdroplets measured from photographs at 13 kV, total count of droplets: 214.

## 4. Conclusions

We developed and tested two optical imaging techniques for measuring sizes of electrosprayed microdroplets in order to control the droplet size distribution when studying plasma-liquid interactions and RONS transport from plasma into water. Theoretically, the detection limit of our double planar laser beam technique for online monitoring of microdroplets is  $\sim 10 \mu\text{m}$ , but we can reliably recognize only droplets with sizes starting from  $\sim 20 \mu\text{m}$ . The camera imaging technique we used for the same electrosprays did not demonstrate a sufficient sensitivity to correlate with size distributions measured by laser beams. We further assume that we can still improve the detection limit of our laser technique if we effectively decrease the width of the detection area by the additional entrance slit from current 3 mm down to 1.5 mm. However, we still need to find suitable independent method to verify the measured distributions.

### Acknowledgments

This work was supported by Slovak Research and Development Agency APVV-17-0382 and Slovak Grant Agency VEGA 1/0419/18, and Faculty of Mathematics, Physics, and Informatics, Comenius University Bratislava.

## 5. References

- [1] Branislav Pongráč: *Study of the Electrospraying Effect of Water in Combination with Atmospheric Pressure Corona Discharge 2014 DOCTORAL THESIS*, Comenius University Bratislava.
- [2] Adamovich I, Baalrud S D, Bogaerts A, et al. 2017 The 2017 Plasma Roadmap: Low temperature plasma science and technology *J. Phys. D. Appl. Phys.* **50** 323001
- [3] Machala Z, Tarabová B, Sersenová D, Janda M and Hensel K 2019 Chemical and antibacterial effects of plasma activated water: correlation with gaseous and aqueous reactive oxygen and nitrogen species, plasma sources and air flow conditions *J. Phys. D. Appl. Phys.* **52** 034002
- [4] Kruszelnicki J, Lietz A M and Kushner M J 2017 *INTERACTION BETWEEN ATMOSPHERIC PRESSURE PLASMAS AND LIQUID MICRO-DROPLETS\** *International Conference on Plasmas with Liquids (ICPL 2017) ed P Lukeš and K Koláček, Prague (Czech Republic), p 37*
- [5] Verlact C C W, Van Boxem W and Bogaerts A 2018 Transport and accumulation of plasma generated species in aqueous solution *Phys. Chem. Chem. Phys.* **20** 6845–59